Journal of Alloys and Compounds 525 (2012) 8–13

Contents lists available at SciVerse ScienceDirect

Journal of Alloys and Compounds

journal homepage: www.elsevier.com/locate/jallcom

# The optical properties of $Eu^{3+}$ and $Tm^{3+}$ codoped $Y_2O_3$ submicron particles

Timur Sh. Atabaev, Hong Ha Thi Vu, Hyung-Kook Kim*, Yoon-Hwae Hwang*

*Department of Nanomaterials Engineering and BK 21 Nano Fusion Technology Division, Pusan National University, Miryang 627-706, Republic of Korea*

ARTICLE INFO

*Article history:*
Received 22 November 2011
Received in revised form 25 January 2012
Accepted 27 January 2012
Available online xxx

*Keywords:*
$Y_2O_3$ particles
Luminescence
Urea homogeneous precipitation
Doping

ABSTRACT

This report presents a fabrication result of nearly uniform-shaped color-tunable $Y_2O_3$ submicron particles codoped with Eu and Tm ions. The resulted particles were characterized by X-ray diffraction, field emission scanning electron microscope and field emission transmission electron microscope, whereas their optical properties were monitored by photoluminescence spectroscopy. The room temperature luminescence emission of synthesized particles was investigated in detail. It was shown that $Eu^{3+}$ and $Tm^{3+}$ codoped $Y_2O_3$ submicron particles exhibits red luminescence (612 nm) under 255 nm excitation, while the emission color of the same particles can be tuned to blue (459 nm) under 320 nm excitation. Different concentrations of $Eu^{3+}$ and $Tm^{3+}$ were induced into the $Y_2O_3$ lattice and the luminescence quenching was observed at high dopant concentrations.



## 1. Introduction

Light is an important component of life. Excitement around the nanofabrication and manipulation of fluorescent materials for applications in life sciences is increasing gradually. Although various fluorescent materials, such as organic dyes and quantum dots (QD), are used widely in life science, they are limited in applications due to the broad spectral features, decomposition, short lifetimes, photo-bleaching and potential toxicity. From this point of view, rare-earth (RE) codoped nanoparticles (NPs) with desirable properties has attracted considerable interest for chemistry, materials science and potential applications in biotechnology. Lanthanide-doped nanoparticles have been recognized as a new promising class of fluorescent materials due to the unique luminescence properties, narrow line-width emission bands, high quantum yields and photostability [1].

The efficiency of RE-doped nanoparticles for frequency conversion is often influenced by the dopant concentration or crystal structure of the host because it changes the phonon frequency [2,3]. The similarity in chemical properties and ionic radius, high melting point (2400 °C) and low cut-off phonon energy (380 $cm^{-1}$) make $Y_2O_3$ a very promising host material for efficient luminescent media. Different RE-doped $Y_2O_3$ NPs have been studied extensively for their unique optical and electronic properties [4–7]. On the other hand, the synthesis methods of RE-doped $Y_2O_3$ particles still require hazardous and toxic reagents. Moreover, the final product is inhomogeneous in size and shape. Non-aggregated phosphor nanoparticles with a spherical morphology were reported to improve the optical performance due to the high packing density and reduction of light scattering [8,9,11]. Therefore, it is very important to design processes that minimize the use and generation of hazardous substances, as well as allow the fabrication of small particles with fine luminescence properties, good crystalline structure and controllable uniform shapes.

Particles with color-tunable emission can be obtained by a combination of some lanthanide ions in the host material. Such a color-tunable nano-phosphorus can find potential applications in display and security printing areas. In our previous report, yttria submicron particles codoped with Eu and Tb activators shows very interesting red-to-green color-tunable luminescent properties [9] depending on the excitation wavelengths. The $Eu^{3+}$ dopant is known as red activator for many host materials [9], while a $Tm^{3+}$ has many 4*f*–4*f* transitions in blue wavelength region [10]. Therefore, $Y_2O_3$ host material codoped with Eu and Tm ions can also show interesting luminescence properties depending on the excitation wavelength. In the present study, easily reproducible, low cost urea homogeneous precipitation method was used to fabricate nearly spherical shaped $Eu^{3+}$ and $Tm^{3+}$ codoped $Y_2O_3$ particles. Luminescence color emission of $Eu^{3+}$ and $Tm^{3+}$ codoped $Y_2O_3$ particles can be tuned precisely by switching the excitation wavelength and is dependent on the dopant ions concentration, which is a parameter easily controlled during fabrication. To the best of author's knowledge, the optical properties of $Y_2O_3$ host material codoped with $Tm^{3+}$ and $Eu^{3+}$ has not been reported so far, motivating the authors to pursue the present work.

* Corresponding authors. Tel.: +82 55 350 5845; fax: +82 55 353 5844.
*E-mail addresses:* hkkim@pusan.ac.kr (H.-K. Kim), yhwang@pusan.ac.kr (Y.-H. Hwang).

0925-8388/$ – see front matter © 2012 Elsevier B.V. All rights reserved.
doi:10.1016/j.jallcom.2012.01.148

## 2. Experimental

### 2.1. Chemical synthesis

Analytical grade yttrium oxide $Y_2O_3$ (99.9%), europium oxide $Eu_2O_3$ (99.9%), thulium oxide $Tm_2O_3$ (99.9%), nitric acid $HNO_3$ (70%) and urea (99–100.5%) were purchased from Sigma–Aldrich and used without a further purification.

Uniform-shaped sub-micron $Eu^{3+}$ and $Tm^{3+}$ codoped $Y_2O_3$ particles were synthesized according to our previous reports [9,11]. In a typical synthesis, yttrium oxide and appropriate amount of rare-earth oxides with a stoichiometric mol ratio (Y/RE = 100 − *x*/*x*, where *x* = 1%Eu–1%Tm; 2%Eu–1%Tm; 3%Eu–1%Tm; 1%Eu–2%Tm; 2%Eu–2%Tm and 3%Eu–2%Tm (a total of 0.001 mol for each sample)) were diluted with nitric acid and vigorously stirred until the solution became colorless. Then the solutions were dried at 70 °C for 1 day to remove the excess nitric acid therein. After cooling down to room temperature, each sample of dried rare-earth salts were mixed with 40 ml of deionized water, 0.5 g of urea and vigorously stirred for 30 min to form a clear solution. Sealed beakers with freshly prepared solutions were then placed into an electrical furnace and heated up to 90 °C for 1.5 h. The resulting colloidal solutions were centrifuged at 5000 rpm for 30 min. The precipitates were washed 3 times with ethanol and DI water and dried at 70 °C for 24 h under vacuum. Dried precipitates were then calcinated in air at 1000 °C for 1 h to produce oxide particles.

### 2.2. Physical characterization

The structure of the prepared powders was investigated via X-ray diffraction (XRD) using a Bruker D8 Discover diffractometer with Cu Kα radiation (λ = 0.15405 nm) within a 2θ scan range of 20–60°. The morphologies of the particles were characterized via field-emission scanning-electron microscopy (FESEM, Hitachi S-4700) and field-emission transmission electron microscopy (FETEM, JEOL JEM-2100F). Elemental analysis was carried out by using energy dispersive X-ray spectroscopy (EDX; Horiba, 6853-H). The PL measurements were performed with a Hitachi F-7000 spectrophotometer equipped with a 150 W Xenon lamp as an excitation source. All the measurements were performed at room temperature.

## 3. Results and discussion

### 3.1. Synthesis, morphology and crystal structure

In the present study, the urea homogeneous precipitation route was utilized to prepare uniform $Eu^{3+}$ and $Tm^{3+}$ codoped $Y_2O_3$ particles. Aqueous solutions of urea are relatively stable under normal conditions. At moderately elevated temperatures, urea decomposes by releasing $NH_3$ and carbonate ions, which cause the subsequent hydrolysis of metals ions present in solution. Since the rate of urea decomposition can be controlled carefully, it is possible to establish conditions that would result in the formation of particles with a uniform size distribution.

An overview synthesis scheme of particles is given through the following reaction steps:

$$RE(NO_3)_3{\cdot}nH_2O + CO(NH_2)_2 \rightarrow RE(OH)CO_3{\cdot}nH_2O + NH_3$$

$$RE(OH)CO_3{\cdot}nH_2O \rightarrow RE_2O_3 + CO_2 + H_2O$$

where RE corresponds to Y, Eu, and Tm.

The collected particles were calcinated at 1000 °C, dispersed in ethanol and sonicated for the TEM observations. For a comparative study of the physical and optical properties, samples with different concentrations of RE codoped ions in $Y_2O_3$ host lattice were synthesized and characterized. Fig. 1 shows that the XRD patterns of synthesized particles belongs to a cubic phase $Y_2O_3$ structure (space group *Ia*3 (206)) with lattice constant *a* = 1.05 nm) [9,11,12]. No additional peaks of other phases have been found, indicating the formation of a purely $Y_2O_3$ cubic phase. It can also

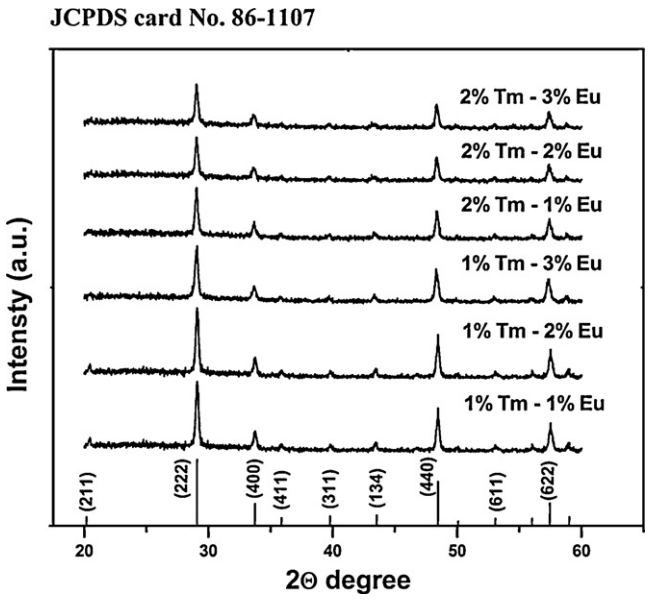


**Fig. 1.** The X-ray diffraction patterns of $Y_2O_3$ particles codoped with different concentrations of $Eu^{3+}$ and $Tm^{3+}$.

be seen that the diffraction peaks of the samples are very sharp and strong, revealing that the final product with high crystallinity can be synthesized by this method. It is very important for phosphors because high crystallinity generally means fewer traps and stronger luminescence [9,11]. The well-known Debye–Scherrer's equation was used to calculate the mean crystallite sizes of samples. Table 1 lists the calculated mean crystallite sizes of synthesized samples. It is known that the emission intensity of phosphor materials depends on the size of the crystallites, i.e., the higher the crystallite size the higher the luminescence intensity. As it will be shown later, the slightly increasing tendency of crystallites can be attributed to the effect of the increased dopant concentration in host material [9], since the luminescence quenching was observed at high dopant concentrations. Fig. 2(a and b) shows the FESEM images of the $Y_2O_3$:1%$Eu^{3+}$–1%$Tm^{3+}$ particles. One can see that particles with sizes of about 150 nm for $Y_2O_3$:1%$Eu^{3+}$–1%$Tm^{3+}$ could be obtained by aging the corresponding RE nitrates solutions for 1.5 h. Doping with different concentrations of Eu and Tm content has almost no effect on the structure and morphology of the final product and the rest of the samples were spherical and similar in sizes (not shown). High resolution FESEM image showed that the $Y_2O_3$:1%$Eu^{3+}$–1%$Tm^{3+}$ particles actually consist of small crystallites, ~50–60 nm in size, which is almost consistent with that estimated by Debye–Scherrer's equation from the XRD patterns. FETEM image of the $Y_2O_3$:1%$Eu^{3+}$–1%$Tm^{3+}$ single particle in Fig. 2(c) confirmed that the samples consist of smaller crystallites associated with each other. HRFETEM showed lattice fringes of 0.305 nm for $Y_2O_3$:1%$Eu^{3+}$–1%$Tm^{3+}$ in Fig. 2 (d), which was assigned to the {2 2 2} crystal plane of the $Y_2O_3$ bcc phase [9–12]. The continuous diffraction rings of $Y_2O_3$:1%$Eu^{3+}$–1%$Tm^{3+}$ in the selective area electron diffraction (SAED) pattern further indicated the crystalline nature of the samples (Fig. 2(e)) [13]. Energy-dispersive X-ray (EDX) spectroscopy of the selected areas revealed the presence of RE ions in the $Y_2O_3$ host (Fig. 2(f)).

**Table 1**
Calculated mean crystallite sizes of $Eu^{3+}$ and $Tm^{3+}$ codoped $Y_2O_3$ particles.

| 1Tm/1Eu | 1Tm/2Eu | 1Tm/3Eu | 2Tm/1Eu | 2Tm/2Eu | 2Tm/3Eu |
|---|---|---|---|---|---|
| 47.61 ± 0.09 | 47.82 ± 0.11 | 47.97 ± 0.10 | 47.79 ± 0.14 | 48.03 ± 0.16 | 48.28 ± 0.07 |

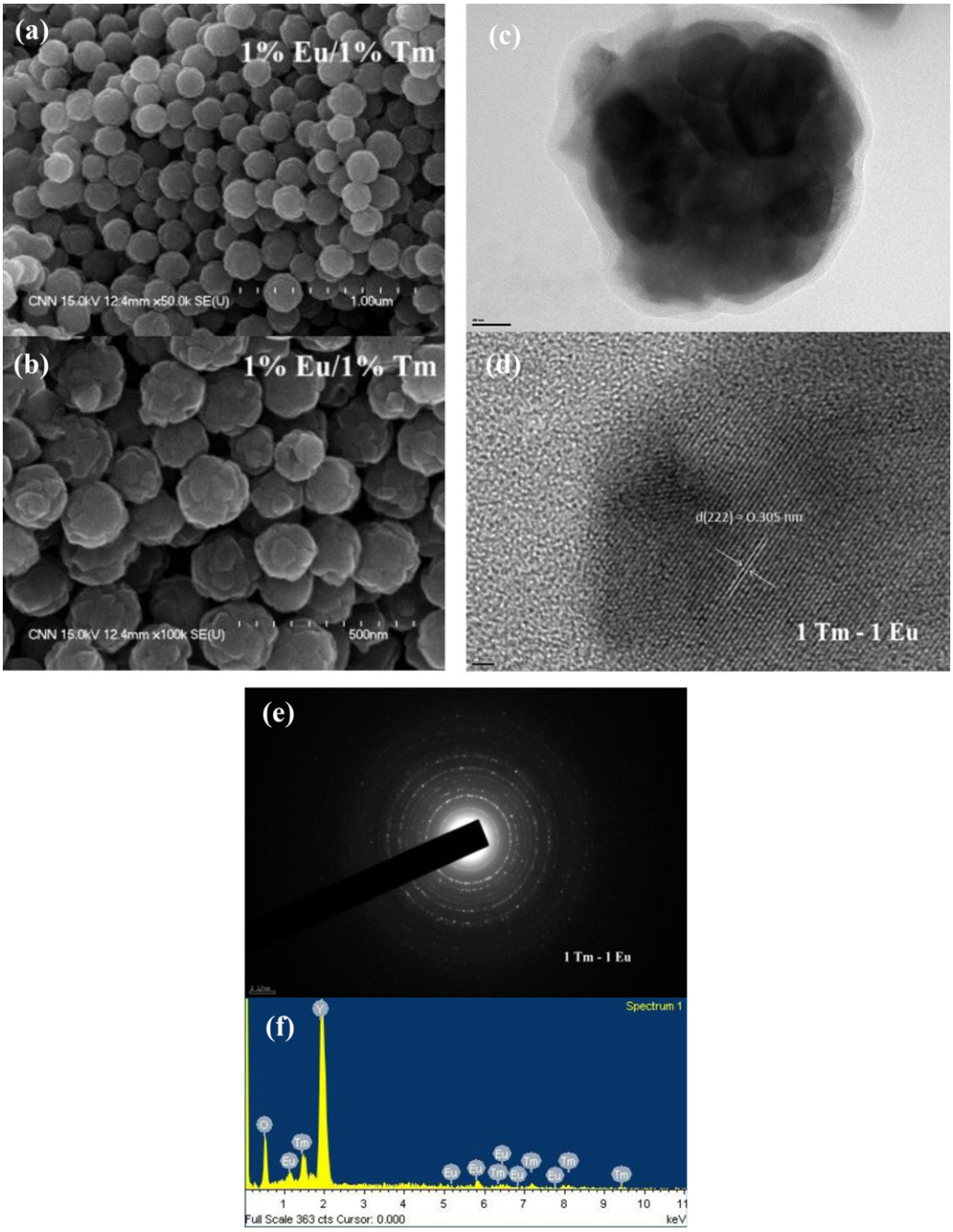


**Fig. 2.** (a) Low magnification and (b) high magnification FESEM images of $Y_2O_3$:1%$Eu^{3+}$–1%$Tm^{3+}$ particles, (c) FETEM image of $Y_2O_3$:1%$Eu^{3+}$–1%$Tm^{3+}$ single particle (scale bar = 40 nm), (d) HRFETEM image of $Y_2O_3$:1%$Eu^{3+}$–1%$Tm^{3+}$ crystal fringes (scale bar = 2 nm), (e) SAED image and (f) EDX spectra of the $Y_2O_3$:1%$Eu^{3+}$–1%$Tm^{3+}$ particles.

### 3.2. Luminescence properties

The concentration of RE ions in the host material is one of the important factors that should be considered during the development of RE-doped phosphor materials. To determine the optimum RE ions doping concentration in the host material, the obtained results were plotted as concentration dependence graphs versus the most intense luminescence peak under a given excitation. Fig. 3(a) shows predominantly red luminescence emission due to $^5D_0 \rightarrow {}^7F_j$ (where j = 0, 1, 2 and 3) $Eu^{3+}$ ion emission transitions in $Y_2O_3$:$Eu^{3+}$–$Tm^{3+}$ systems under 255 nm excitation. On the other hand, a weak blue $^1G_4 \rightarrow {}^3H_6$ transition in $Y_2O_3$:$Eu^{3+}$–$Tm^{3+}$ was also detectable. A close examination of the most intense characteristic peak at 612 nm assigned to a $^5D_0 \rightarrow {}^7F_2$ transition showed that the intensity increased with increasing Eu content and reached a maximum when the concentration was 2 mol.% and then decreased at higher concentrations in $Y_2O_3$:1$Tm^{3+}$–x$Eu^{3+}$ samples (Fig. 3(b)). In contrast to the $Y_2O_3$:1$Tm^{3+}$–x$Eu^{3+}$ samples, the luminescence intensity of $Y_2O_3$:2$Tm^{3+}$–x$Eu^{3+}$ particles showed the downward trend under the same 255 nm excitation (Fig. 3(b)). The emitting color of $Y_2O_3$:$Eu^{3+}$–$Tm^{3+}$ systems can be tuned to blue under 320 nm excitation, which is due to the $^1G_4 \rightarrow {}^3H_6$ and $^1D_2 \rightarrow {}^3F_4$ transitions within the Tm ions, however, weak red characteristic $^5D_0 \rightarrow {}^7F_j$ transitions of $Eu^{3+}$ were also observed as shown in Fig. 4(a). One can see that in contrast to Eu ions, Tm ions were found to be concentration-sensitive to the presence of Eu codoped ions. Hence, their corresponding most intense peaks (459 nm for $Tm^{3+}$) decreased significantly with increasing of any (Eu or Tm) dopant

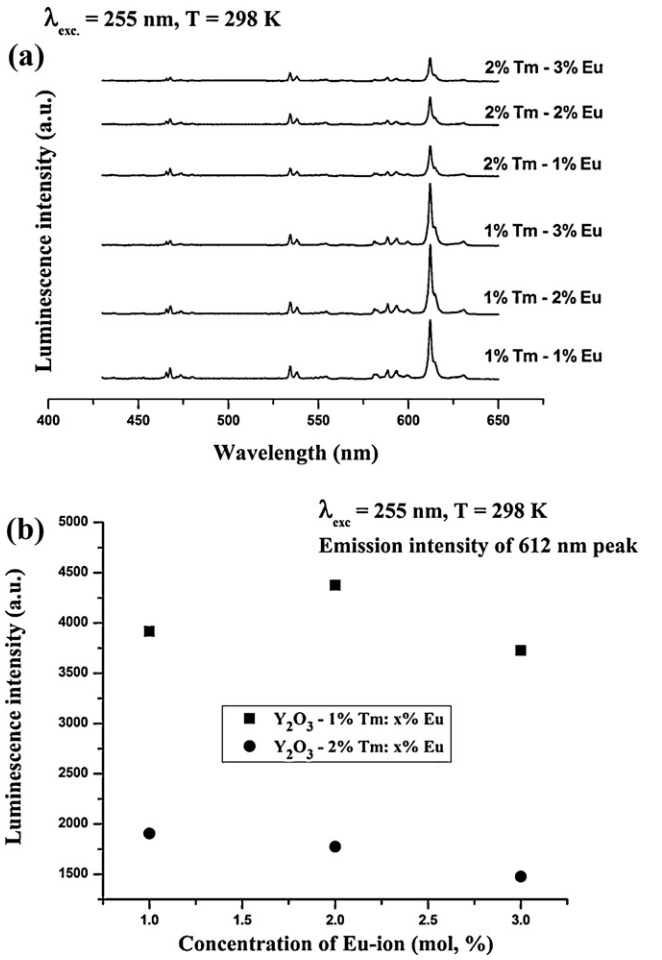


**Fig. 3.** (a) PL emission spectra of $Y_2O_3$ particles codoped with different concentrations of $Eu^{3+}$ and $Tm^{3+}$ upon 255 nm excitation. (b) The integrated emission intensity of 612 nm peaks of $Y_2O_3$ particles codoped with different concentrations of Eu and Tm ions.

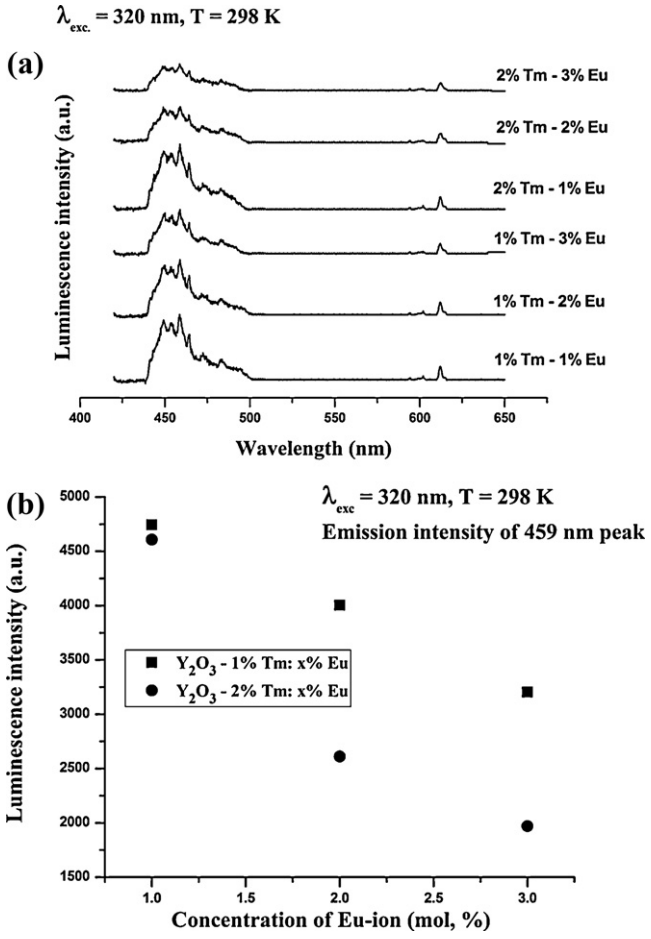


**Fig. 4.** (a) PL emission spectra of $Y_2O_3$ particles codoped with different concentrations of $Eu^{3+}$ and $Tm^{3+}$ upon 320 nm excitation. (b) The integrated emission intensity of 543 nm peak of $Y_2O_3$ particles codoped with different concentrations of Eu and Tm ions.

ions concentration in the host (Fig. 4(b)). This highlights the effect of concentration quenching on the luminescence properties in this host. The most reasonable explanation for this concentration-quenching behavior is cross-relaxation between RE-ions because a higher dopant concentration leads to a decrease in the average distance between dopant ions, and to the formation of dopant pairs or clusters in some cases. This then promotes an interaction between ions, energy migration, and non-radiative cross-relaxation processes to the ground state [9,11], which finally results in quenching of the luminescence intensity.

The excitation spectra of $Y_2O_3$:1%$Eu^{3+}$–1%$Tm^{3+}$ shown in Fig. 5. It is well known that upon excitation into charge-transfer-band CTB of the Eu–O at 255 nm the emission spectrum exhibits several group of emission lines, which are ascribed to the $^5D_0 \rightarrow {}^7F_j$ (where j = 0, 1, 2 and 3) transitions of $Eu^{3+}$ (Fig. 3(a)) [9]. Fig. 6 represented the schematic energy level diagram and the observed luminescence transitions in the $Y_2O_3$:$Eu^{3+}$–$Tm^{3+}$ systems. The existence of broad band in the range of 275–385 nm which is related to Tm–O charge transfer [14] (Fig. 5), shows that the some energy transfers also to Tm ions, therefore weak blue $^1G_4 \rightarrow {}^3H_6$ transition within the Tm ions also detectable. The direct excitation of Tm–O charge transfer band at 320 nm give rise to $^1G_4 \rightarrow {}^3H_6$ and $^1D_2 \rightarrow {}^3F_4$ transitions within the Tm ions with feeble energy transfer from Tm to Eu ions. Therefore, it can be concluded that the energy transfer between the codoped $Tm^{3+}$ and $Eu^{3+}$ is not sufficient in contrast to previously reported $Tb^{3+} \rightarrow Eu^{3+}$ energy transfer in $Y_2O_3$ [9,15].

Fig. 7 shows the emission spectra of $Y_2O_3$:1%$Eu^{3+}$–1%$Tm^{3+}$ (particles with lower dopant concentrations) upon 255 and 320 nm excitations respectively. Inset digital images show the eye-visible red and blue emissions from $Y_2O_3$:1%$Eu^{3+}$–1%$Tb^{3+}$ particles upon different excitation wavelengths. The light output manipulation of phosphor material can be useful in many practical applications,

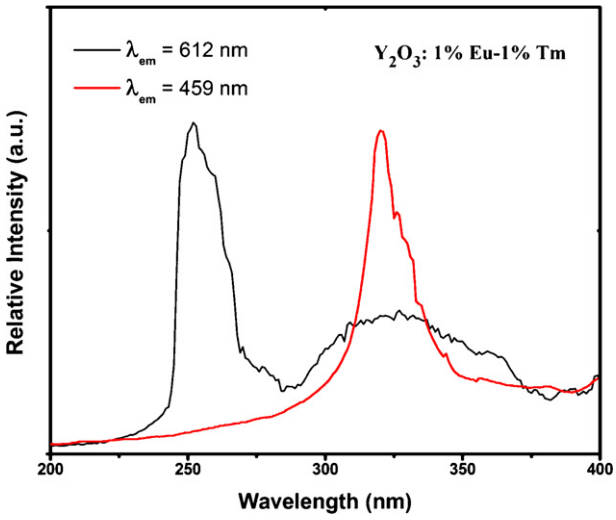


**Fig. 5.** The excitation spectra of the $Y_2O_3$:1%$Eu^{3+}$–1%$Tm^{3+}$ phosphor particles.

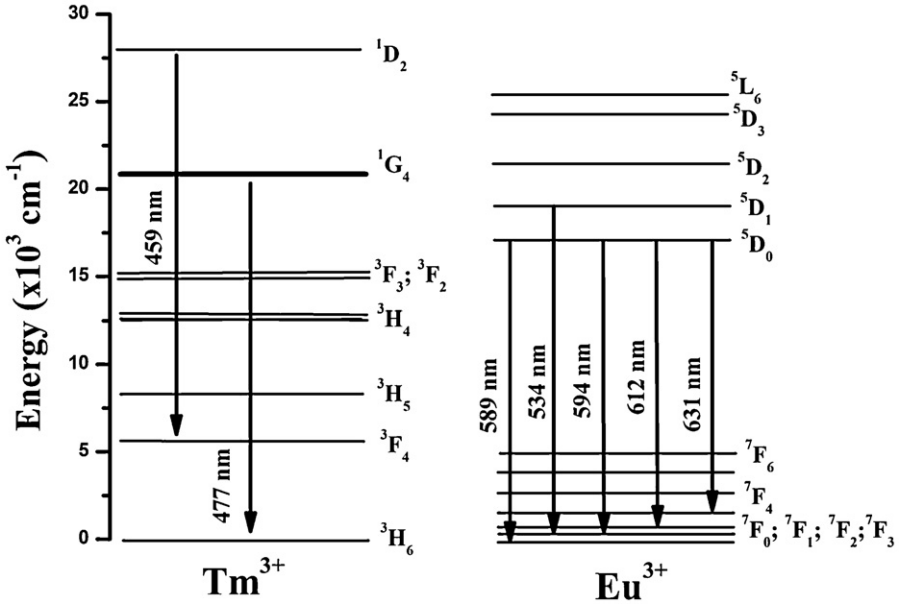


**Fig. 6.** Schematic diagram illustrating the $Tm^{3+}/Eu^{3+}$ energy band structure and Stokes transitions between the levels.

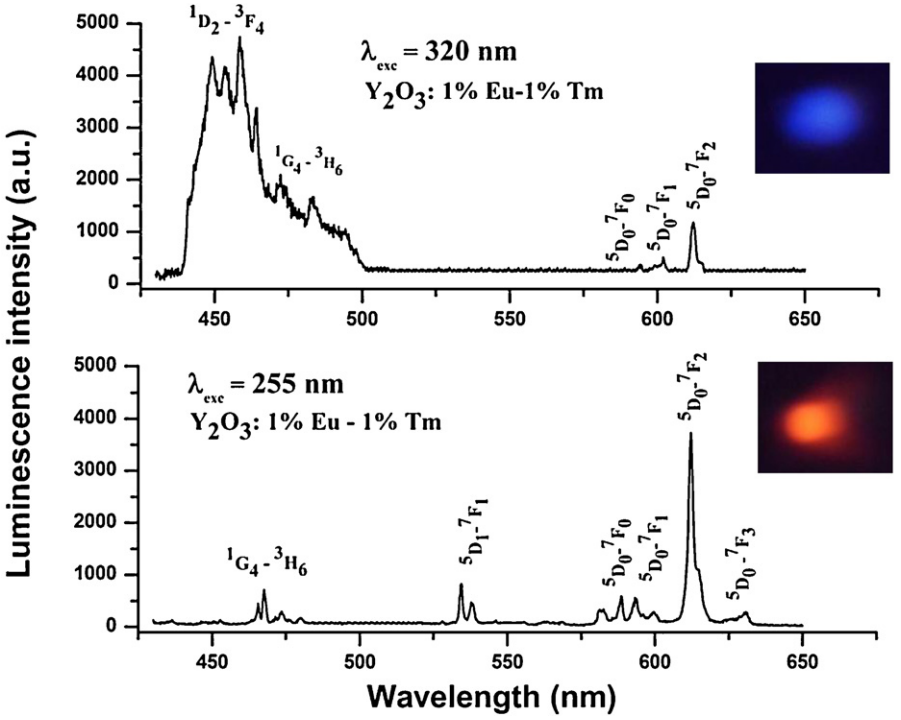


**Fig. 7.** PL emission of $Y_2O_3$:1%$Eu^{3+}$–1%$Tm^{3+}$ particles upon excitation at 255 and 320 nm. Inset shows digital photographs of eye-visible red and blue luminescence emission.

for example in solid state illumination, security-printing area, and other related areas.

## 4. Conclusion

In summary, nearly spherical $Y_2O_3$ sub-micron particles codoped with Eu/Tm ions were synthesized via cost-effective and user-friendly urea homogeneous precipitation. A combination of Eu/Tm ions in a single yttrium oxide host material allows to manipulate the luminescence color output in phosphor material upon excitation of different wavelengths. In $Eu^{3+}$ and $Tm^{3+}$ codoped yttria particles, Tm ions are found to be concentration-sensitive and corresponding blue luminescence peak was quenched significantly with increasing of codoped rare-earth ions concentration in the host. Fine color-tunable luminescence emission may find many potential applications, including display panels, security printing, solid-state illumination, etc.

## Acknowledgements

This work was supported by the National Research Foundation of Korea (NRF) funded by the Ministry of Education, Science and Technology (No. 2010-0010575). The authors would like to thank

Prof. J. B. Lee for allowing the use of his equipment for the preparation and characterization of samples.

## References

[1] Y. Wang, R.X. Yan, Z.Y. Hao, L. Wang, J.H. Zeng, H. Bao, X. Wang, Q. Peng, Y.D. Li, Angew. Chem. Int. Ed. 44 (2005) 6054–6057.
[2] T.Sh. Atabaev, Z. Piao, H.K. Kim, Y.H. Hwang, B.K. Kim, J. Nanosci. Nanotechnol. 11 (2011) 5892–5897.
[3] A. Patra, C.S. Friend, R. Kapoor, P.N. Prasad, Chem. Mater. 15 (2003) 3650.
[4] S. Chandra, F.L. Deepak, J.B. Gruber, D.K. Sardar, J. Phys. Chem. C 114 (2010) 874–880.
[5] H. Guo, Y.M. Qiao, Opt. Mater. 31 (2009) 583–589.
[6] J.-L. Yuan, Z.-Y. Zeng, J.-T. Zhao, Z.-J. Zhang, H.-H. Chen, X.-X. Yang, J. Phys. D: Appl. Phys. 41 (2008) 105406.
[7] X. Yang, S. Xiao, Z. Liu, X.H. Yan, Appl. Phys. B 86 (2007) 77–82.
[8] Y.C. Kang, I.W. Lenggoro, S.B. Park, K. Okuyama, J. Phys. Chem. Solids 60 (1999) 1855–1858.
[9] T.Sh. Atabaev, H.K. Kim, Y.H. Hwang, J. Colloid Interface Sci., doi:10.1016/j.jcis.2011.09.047, in press.
[10] A. Fukabori, V. Chani, K. Kamada, F. Moretti, A. Yoshikawa, Cryst. Growth Des. 11 (2011) 2404–2411.
[11] T.Sh. Atabaev, H.-H. Vu Thi, Y.-D. Kim, J.-H. Lee, H.-K. Kim, Y.-H. Hwang, J. Phys. Chem. Solids 73 (2012) 176–181.
[12] F. Zhang, G.B. Braun, Y. Shi, Y. Zhang, X. Sun, N.O. Reich, D. Zhao, G. Stucky, J. Am. Chem. Soc. 132 (2010) 2850–2851.
[13] M. Jayasimhadri, B.V. Ratnam, K. Jang, H.S. Lee, B. Chen, S.-S. Yi, J. Jeong, L. Rama Moorthy, J. Am. Ceram. Soc. 93 (2) (2010) 494–499.
[14] M.N. Luwang, R.S. Ningthoujam, S.K. Srivastava, R.K. Vatsa, J. Mater. Chem. 21 (2011) 5326.
[15] S. Mukherjee, V. Sudarsan, R.K. Vatsa, S.V. Godbole, R.M. Kadam, U.M. Bhatta, A.K. Tyagi, Nanotechnology 19 (2008) 325704.